

Article

Theoretical Study of Complexes of Tetravalent Actinides with DOTA

 Attila Kovács 

Joint Research Centre (JRC), European Commission, P.O. Box 2340, 76125 Karlsruhe, Germany; attila.kovacs@ec.europa.eu

Abstract: 1,4,7,10-Tetraazacyclododecane- N,N',N'',N''' -tetraacetic acid (H_4 DOTA) is a prominent chelating ligand with potential applications in various fields, from radiotherapy to the separation of fission products. The present study explores the stability, structure, and bonding properties of its complexes with tetravalent actinides ($An = Th, U, Np, Pu$) using density functional theory and relativistic multireference calculations. Neutral complexes prefer to form symmetric (C_4) structures with DOTA. The first coordination sphere of the actinide ions is readily saturated by a weakly bonded H_2O ligand. The latter ligand reduces the molecular symmetry while exerting only marginal effects on the properties of the parent complex. An-ligand bonding is mainly electrostatic, but there are also significant charge-transfer contributions from DOTA to the An 6d/5f orbitals. The charge-transfer interactions and the covalent character of bonding increase gradually in the order of $Th < U < Np < Pu$, as indicated by analysis of the electron density distribution using the Quantum Theory of Atoms in Molecules.

Keywords: actinides; DOTA; bonding; DFT; QTAIM



Citation: Kovács, A. Theoretical Study of Complexes of Tetravalent Actinides with DOTA. *Symmetry* **2022**, *14*, 2451. <https://doi.org/10.3390/sym14112451>

Academic Editors: Takashiro Akitsu and Brijesh M. Sharma

Received: 27 October 2022

Accepted: 15 November 2022

Published: 18 November 2022

Publisher's Note: MDPI stays neutral with regard to jurisdictional claims in published maps and institutional affiliations.



Copyright: © 2022 by the author. Licensee MDPI, Basel, Switzerland. This article is an open access article distributed under the terms and conditions of the Creative Commons Attribution (CC BY) license (<https://creativecommons.org/licenses/by/4.0/>).

1. Introduction

1,4,7,10-Tetraazacyclododecane- N,N',N'',N''' -tetraacetic acid (H_4 DOTA) is an efficient chelating agent that forms stable metal complexes, particularly with f elements [1]. This stability is based on strong interactions with the four pendant carboxylate arms in addition to the four nitrogen donors of the cyclen moiety (Figure 1), facilitating octadentate maximal coordination with deprotonated DOTA. The advantageous size of the macrocyclic cavity is an additional important issue.

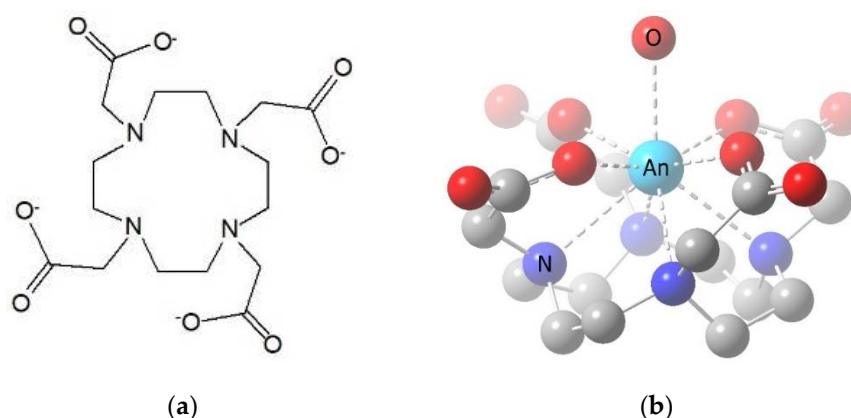


Figure 1. (a) Schematic drawing of the DOTA⁴⁻ ligand; (b) The C_4 SAP structure of the $Th(DOTA)(H_2O)$ complex, gradually faded towards the back. Hydrogen atoms of the ligands are omitted for clarity.

Due to their high thermodynamic stability and kinetic inertness in physiological conditions, DOTA complexes have been used for several medical applications. The Gd^{III} complex is the active substance of the MRI contrast agent Dotarem [2,3], and the Eu^{III} , Tm^{III} , and Yb^{III} complexes of DOTA derivatives were probed for paramagnetic chemical exchange saturation transfer (PARACEST) agents [4–6]. DOTA complexes with α -emitting radioisotopes (^{213}Bi , ^{225}Ac , ^{227}Th) found an application in targeted α -therapy (TAT) [7–9], showing remarkable efficiency for treating metastatic castration-resistant prostate cancer [10–12], acute myeloid leukemia [13,14], and neuroendocrine tumours [15]. In addition to the abovementioned ^{213}Bi and ^{225}Ac radionuclides, DOTA is the primary choice for chelating β -emitting ^{177}Lu isotopes for applications in radiotherapy [16].

Though the complexes of DOTA with trivalent metals have been studied extensively [1,17–19], largely due to the above applications, less attention has been paid to complexes with tetravalent metals. This oxidation state is favourable for several early actinides (An = Th, U, Np, Pu), and with this ligand, very stable complexes can be expected. Relevant literature includes the report on oligomers from dimers to hexamers in a solid-state and aqueous solution (An = Th, U, Np, Pu) [20]. Under appropriate conditions, the monomers $Th(\kappa^8\text{-DOTA})(DMSO)$ and $U(\kappa^8\text{-DOTA})(DMSO)$ could be prepared and crystallographically characterised [21]. This has been followed by a study of the redox behaviour of the monomeric $U^{IV}(\text{DOTA})$ complex in aqueous solution [22].

The aim of the present study is a comparative analysis of DOTA complexes with tetravalent An (Th, U, Np, Pu) and an attempt to shed light on the stability and bonding properties by means of quantum chemical calculations. The metal–ligand interactions are analysed by the Quantum Theory of Atoms in Molecules (QTAIM) [23–25] and the Extended Transition State method combined with the Natural Orbitals of Chemical Valence (ETS-NOCV) [26] models.

2. Computational Details

Density Functional Theory (DFT) computations were performed with the Gaussian09 suit of programs [27]. On the basis of a good reported performance for the molecular geometries and relative stabilities of various *f*-element complexes [19,28–31], the TPSSh meta-hybrid functional [32] was applied. For the actinides, the 5*f*-in-valence (small-core) quasi-relativistic pseudopotentials of the Stuttgart-Cologne group (ECP60MWB) [33,34] were used in conjunction with segmented valence basis sets of triple-zeta quality (contraction scheme (14s13p10d8f6g)/(10s9p5d4f3g)) [34,35], whereas for the light atoms, the standard 6-311 + G** basis was applied. Test calculations with the 5*f*-in-core (large-core) pseudopotentials (Th-ECP78MWB, U-ECP80MWB, Np-ECP81MWB, Pu-ECP82MWB [36]) were also performed in conjunction with the contracted (7s6p5d2f)/(5s4p4d2f) valence basis for the actinides [36] and the 6-311+G** basis for light atoms. This latter theoretical level resulted in unreasonable metal–ligand distances for the Th complexes and was therefore omitted from the further study.

In order to account for dispersion effects, the D3 version of Grimme's empirical correction using Becke–Johnson damping (GD3BJ) [37] was utilised. As it is important for weak interactions, the SuperFine grid was applied for integration accuracy. It contains 150 radial shells and 974 angular points per shell for C, N, and H and 225 radial shells for An. The ground states of the computed complexes were verified using the STABLE keyword of the Gaussian09 code. In order to be consistent with earlier studies [19,28–31], geometry optimisations and other computations were performed for the isolated molecules (gaseous phase).

The multiconfigurational natures of the U, Np, and Pu complexes were assessed by single-point relativistic complete active space self-consistent field (CASSCF) calculations [38]. These single-point calculations were performed on the TPSSh optimised geometries, taking advantage of their symmetry. This study verified the ground electronic state of each complex and their characters. The calculations were carried out by means of

the MOLCAS 8.2 code [39,40] in frame of the C_2 point group, the highest applicable one for these complexes.

The scalar relativistic effects were taken into account using the second-order Douglas–Kroll–Hess Hamiltonian [41,42]. All-electron basis sets of atomic natural orbital type, developed for relativistic calculations (ANO-RCC), were used with valence double-zeta plus polarization contraction schemes of (26s23p17d13f5g3h)/(8s7p5d3f1g) for An [43], (8s4p3d1f)/(2s1p) for H [44], and (14s9p4d3f2g)/(3s2p1d) for C, N, and O [45]. Due to the large size of the complexes, the active space consisted of the seven 5f orbitals occupied by the 5f electrons of the An^{4+} ions. Because the bonding orbitals containing An–ligand interactions were found to have relatively low energies (below those of the O lone pairs), they had no relevance for the active space. This was confirmed by test calculations with active spaces up to 18 electrons on 16 orbitals for the U(DOTA)(H₂O) complex.

Spin–orbit (SO) effects were taken into account by utilising the complete active space state interaction (CASSI) method [46], which allows CASSCF wave functions for different electronic states to interact under the influence of a spin–orbit Hamiltonian. In the state-averaged calculations, all the states of the ground-state spin multiplicities were considered, i.e., 21, 35, and 35 roots for U, Np, and Pu, respectively.

A bonding analysis was performed on the basis of the TPSSh wave functions with the Multiwfn code [47]. The Bader atomic charges, delocalisation indices, and topological properties in terms of the Quantum Theory of Atoms in Molecules (QTAIM) [23,25] were evaluated using a medium-quality grid.

3. Results and Discussion

3.1. Geometrical Characteristics

The DOTA ligand consists of a twelve-membered tetraaza (cyclen) ring and four pendant carboxylate arms. Metal ions can be coordinated by the four N atoms of cyclen and the four O atoms of the COO[−] arms. In addition, with large metals, there is sufficient free space for a ninth coordination, e.g., by an H₂O molecule (cf. Figure 1). This is the usual coordination of heavy metals, including the lanthanides (Ln) and An [48–55]. In contrast, complex formation with the smaller Ca, Bi, and Sc is managed with a coordination number of CN = 8 [49,56,57], whereas even smaller transition metals are coordinated only by the four N atoms and two or three carboxylate groups (CN = 6, 7) [50,58–60].

The DOTA complexes have an interesting stereochemistry. One stereochemical element is the cyclen moiety, in which the four metal–N interactions fix the four ethylene groups either in a δ - or a λ -gauche orientation ($\delta\delta\delta\delta$ or $\lambda\lambda\lambda\lambda$, respectively). The second stereochemical element corresponds to the two possible opposite helical arrangements (Δ and Λ) of the four COO[−] groups. As a consequence, the octacoordinated complexes can appear as two diastereoisomeric pairs of enantiomers [18]. They are $\Lambda(\delta\delta\delta\delta)/\Delta(\lambda\lambda\lambda\lambda)$, whereby the ring and the arms have opposite helicities, and $\Delta(\delta\delta\delta\delta)/\Lambda(\lambda\lambda\lambda\lambda)$, whereby the ring and acetate groups have identical helicity. The former diastereomers have a square antiprismatic structure (designated as SAP or M in the literature), and the latter ones have a twisted square antiprismatic geometry (designated as TSAP or m).

Crystal structure studies revealed that the complexes of Ln from Pr to Lu adopt the SAP structure [48–51,61], whereas the complexes with the larger La [55] and Ce [49] adopt the TSAP structure. In solutions of Ln^{III}(DOTA)[−] complexes, mixtures of the two conformers were found by NMR spectroscopy [62,63]. The ratio of the SAP and TSAP forming across the Ln row varies according to the trend observed in the crystals (vide supra). The H₂O ligand at the ninth coordination site is involved in a rapid exchange process with the solvent H₂O molecules [64,65].

Whereas no experimental structural data are available for An^{III}(DOTA) complexes, recent DFT calculations modelling the aqueous solution predicted the preference of the TSAP conformer for trivalent An = Ac [19,66,67] and U–Cf [19]. In contrast, the recently reported solid-state structures of U^{IV}(DOTA) with DMSO [21] and F additional ligands at the ninth coordination site [22] corresponded to the SAP conformer in both the crystal and

aqueous solution. This changed structural preference is in agreement with the smaller ionic radius of U^{IV} vs. U^{III} by 0.135 Å [68]. (The ionic radius of U^{4+} agrees with that of Er^{3+} , the latter known to prefer SAP, *vide supra*.) Based on the preference of the SAP conformer for U^{IV} (DOTA) complexes [21,22], the theoretical analyses performed here are restricted on these isomers of the Th^{IV} , U^{IV} , Np^{IV} , and Pu^{IV} complexes.

In agreement with the structure model applied for An^{III} (DOTA)(H_2O)[−] complexes in Ref. [19], the H_2O molecule was constrained in a vertical arrangement facilitating C_2 symmetry. According to the frequency analysis, this structure is a first-order saddle-point on the potential energy surface. However, due to the very weak An–OH₂ interaction, it is only marginally higher in energy than the global minimum. Moreover, this arrangement is expected to resemble those in the solid-state and polar solvents, in which the H_2O ligand is involved in interactions with the environment rather than with the DOTA ligand in the same complex (the latter happening in the global minimum of the computed isolated molecule).

The bond distance data depicted in Figure 2 reveal an excellent correlation between the An^{4+} effective ionic radii [68] and the computed An–O and An–N bond distances in the An^{IV} (DOTA) complexes. The H_2O ligand at the ninth coordination site has a small influence on the An–DOTA interaction, manifested in a slight increase (0.02–0.03 Å) in the An–O and An–N bond distances. Due essentially to the neutral nature of the H_2O ligand, it is bonded considerably weaker to An^{IV} than the anionic carboxylate oxygens: the An–O_{H₂O} bonds are longer by ca. 0.2 Å than the An–O bonds with DOTA. These An–O_{H₂O} bonds do not follow the An^{4+} ionic radii (as often observed for weaker bonded secondary ligands). In addition to the weak bonding forces, the position of H_2O may suffer from electrostatic repulsion with the adjacent carboxylate arms (cf. Figure 1).

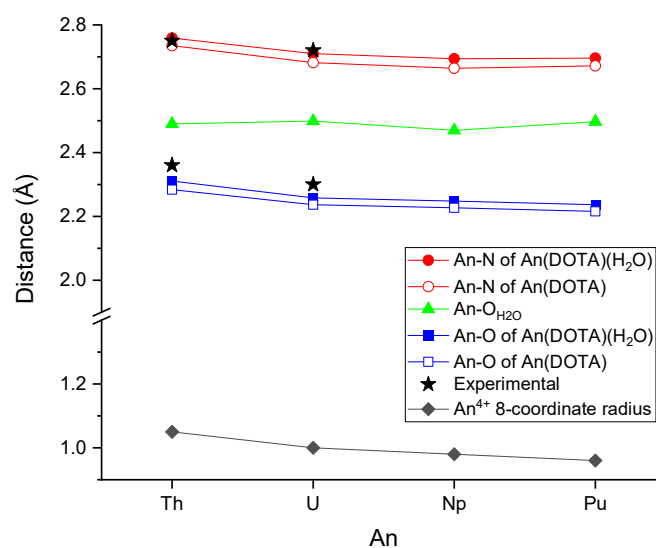


Figure 2. Comparison of computed and experimental [21] An–O and An–N bond distances of the An^{IV} (DOTA) complexes, as well as the An^{4+} 8-coordinate effective ionic radii [68]. The slightly different computed values originating from the C_2 symmetry of An (DOTA)(H_2O) structures are averaged. The presented values are given in Table S1 of the Supplementary Materials.

The computed An–O and An–N distances can be compared to related experimental X-ray diffraction structural data of the Th^{IV} (DOTA)(DMSO) and U^{IV} (DOTA)(DMSO) complexes [21] in Figure 2 (see also Table S1 of the Supplementary Materials). Whereas the An–N data show an excellent agreement, the computed An–O values are slightly underestimated. The latter relations are consistent with the larger steric effect of the DMSO ligand compared to H_2O , positioned near the coordinating carboxylate groups.

Another characteristics of the geometrical parameters of the title complexes are the distances of An from the planes of the O and N donors presented in Figure 3. They give the

position of An within the cavity of DOTA and show how it characteristically changes upon the additional (H_2O , DMSO) ligands at the ninth coordination site.

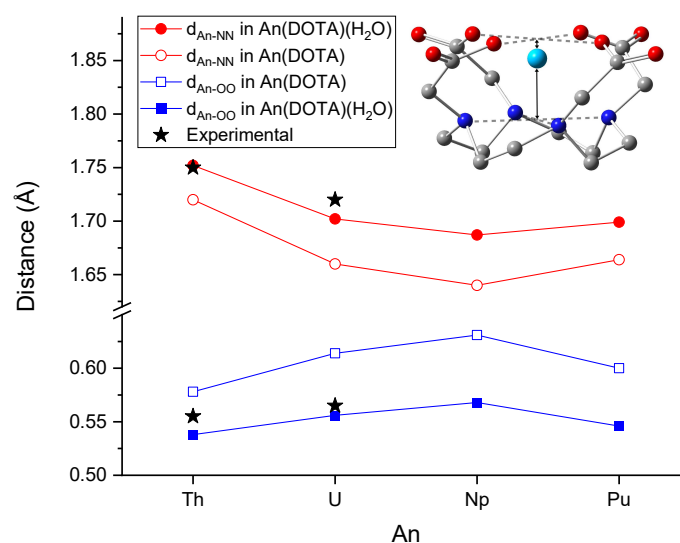


Figure 3. Comparison of computed and experimental [21] distances of An to the planes of the O and N donors (defined by the midpoints of the $\text{O} \cdots \text{O}$ and $\text{N} \cdots \text{N}$ lines, see insert) in the complexes. The different values originating from the C_2 symmetry of $\text{An}(\text{DOTA})(\text{H}_2\text{O})$ structures are averaged. The presented values are given in Table S2 of the Supplementary Materials.

First, the excellent agreement of the computed $\text{An}(\text{DOTA})(\text{H}_2\text{O})$ data with the X-ray diffraction results on the $\text{An}(\text{DOTA})(\text{DMSO})$ complexes should be noted. This agreement is somewhat better than that of the An–O and An–N bond distances in Figure 2 (vide supra).

Figure 3 demonstrates that An is significantly closer (by ca. 1 Å) to the plane of the O donors than to the plane of the N donors, whereas the An–O and An–N distances differ only by ca. 0.5 Å. The feature is based on the larger radius of the donor O shell, and its consequence is the possibility of a ninth coordination site available for small ligands, such as H_2O in aqueous solution. The H_2O (and DMSO in Ref. [21]) ligands pull An further away from the plane of the N shell.

The change of the DOTA cavity in the complexes along the An row is also represented by the curves in Figure 3. The gradual decrease in the An–O and An–N bond distances in Figure 2 is manifested only in the An–NN distances from Th to Np. Hence, in these complexes, An moves gradually towards the donor N shell, away from the donor O shell. This trend is reversed in the Pu complex, implying a relative strengthening of the Pu–O interactions as compared to the other three An. This slightly out-of-trend effect can be recognised in the properties of covalent metal–ligand interactions (vide infra).

Another notable observation from these data is the strong deformation from C_4 symmetry at the carboxylate site of the $\text{An}(\text{DOTA})(\text{H}_2\text{O})$ complexes, as reflected by the significantly different distances from the individual O donors (Table S2). In contrast, the effect on the An–N contacts is negligible.

3.2. Electronic Structure

In order to verify the multiconfigurational nature in the complexes, CASSCF calculations with active spaces consisting of the 5f orbitals were performed on the $\text{An}(\text{DOTA})$ and $\text{An}(\text{DOTA})(\text{H}_2\text{O})$ molecules with An = U, Np, Pu (as the Th^{4+} ion has no 5f electrons). Selected characteristics of the spin–orbit (SO) and spin–orbit-free (SF) ground states are compiled in Table 1.

Table 1. Selected characteristics of the spin–orbit (SO) and spin–orbit-free (SF) ground states of An(DOTA) and An(DOTA)(H₂O) complexes from CASSCF calculations.

Complex	State ¹	SO Composition (%) ²	SF Composition (%) ³
U(DOTA)	³ H ₄	³ A (42) + ³ B (26) + ³ B (26)	³ A (93)
Np(DOTA)	⁴ I _{9/2}	⁴ A (40) + ⁴ B (20) + ⁴ B (20)	⁴ A (85)
Pu(DOTA)	⁵ I ₄	⁵ A (38) + ⁵ A (32)	⁵ A (88)
U(DOTA)(H ₂ O)	³ H ₄	³ A (40) + ³ B (30) + ³ B (23)	³ A (91)
Np(DOTA)(H ₂ O)	⁴ I _{9/2}	⁴ A (32) + ⁴ B (27) + ⁴ B (13)	⁴ A (86)
Pu(DOTA)(H ₂ O)	⁵ I ₄	⁵ A (29) + ⁵ A (23) + ⁵ B (12)	⁵ A (85)

¹ Term symbol of the electronic state of An⁴⁺ in the complexes. ² Composition of the SO ground state from the SF states (lowest-energy C₂ irreducible representations). ³ Symmetry of the SF ground state and the %-contribution of the main electron configuration in it.

The term symbols of the obtained SO ground electronic states of An in the complexes agree with those of the free An⁴⁺ ions [69–71]. The SO ground states of the present complexes consist generally of mixtures of the lowest-energy SF states. In the case of the Pu complexes, the major contributions belong to the A irreducible representation of the C₂ point group, whereas in the U and Np complexes, they belong to both the A and B symmetries in comparable magnitude. This is due to the very close energies of the lowest-energy states of the two symmetry groups in the latter cases. On the other hand, the SF ground electronic states belong to symmetry A for all the six complexes (and for the non-multiconfigurational Th complexes too).

The SF ground states contain mostly one dominant (85–93%) electron configuration. These major electron configurations are generally strongly mixed and cannot be characterised by specific magnetic quantum numbers of the 5f electrons. Nevertheless, comparison with the Mulliken populations of the 5f orbitals from the DFT calculations revealed a fair qualitative agreement between the two computational levels, supporting in this way the reasonability of the ground electronic states from DFT.

3.3. Bonding

The metal–ligand interactions in the complexes are characterised by the Wiberg bond indices [72] and selected QTAIM [23,25] parameters. From the latter parameters, the Bader atomic charges provide the main information on the ionic interactions and the charges transferred (CT) from the ligands to An. The An charges are given in Table 2, and the CT data from TPSSH calculations are depicted in Figure 4.

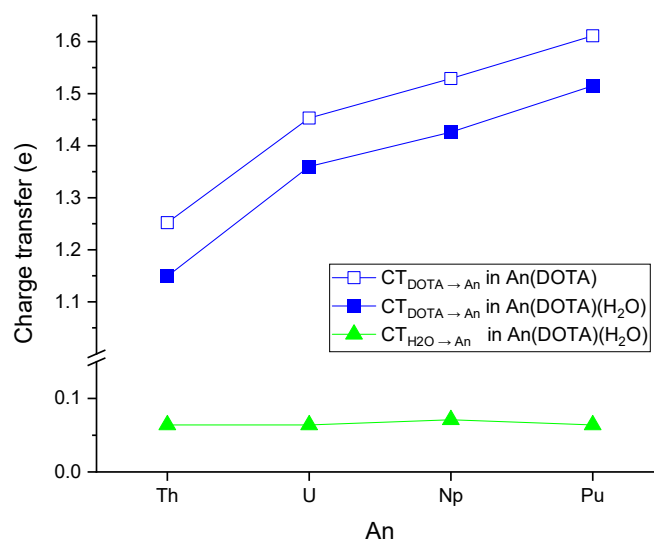
**Figure 4.** Charge transfer (e) data in the complexes. The presented values are given in Table S3 of the Supplementary Materials.

Table 2. Selected results from the DFT-based QTAIM analysis of An(DOTA) and An(DOTA)(H₂O) complexes ¹.

An	q _{An}	$\rho(r)$			$\nabla^2\rho(r)$			H(r)			ϵ		
		An-O	An-N	An-O _w	An-O	An-N	An-O _w	An-O	An-N	An-O _w	An-O	An-N	An-O _w
Th(DOTA)	2.75	0.086	0.041		0.277	0.105		−0.016	−0.003		0.08	0.02	
U(DOTA)	2.55	0.092	0.043		0.317	0.118		−0.017	−0.003		0.07	0.09	
Np(DOTA)	2.47	0.093	0.043		0.338	0.126		−0.017	−0.003		0.04	0.09	
Pu(DOTA)	2.39	0.094	0.042		0.353	0.121		−0.016	−0.003		0.02	0.06	
Th(DOTA)(H ₂ O)	2.79	0.080	0.039	0.051	0.265	0.101	0.199	−0.013	−0.002	0.000	0.08	0.02	0.16
U(DOTA)(H ₂ O)	2.58	0.087	0.041	0.047	0.304	0.112	0.198	−0.015	−0.003	0.000	0.09	0.07	0.12
Np(DOTA)(H ₂ O)	2.50	0.088	0.041	0.049	0.323	0.118	0.205	−0.014	−0.003	0.000	0.03	0.11	0.06
Pu(DOTA)(H ₂ O)	2.42	0.089	0.039	0.047	0.335	0.116	0.193	−0.014	−0.002	0.000	0.02	0.05	0.12

¹ From TPSSh-GD3BJ/ECP60MWB+TZP calculations. Bader charge of An (q_{An}, e); averaged electron density ($\rho(r)$, au), Laplacian of this electron density ($\nabla^2\rho(r)$, au), total electronic energy density (H(r), au), and ellipticity of electron density distribution (ϵ , au) at the An–O and An–N bond critical points. O_w in the heading means O_{H₂O}.

The charges of the An ions are highly positive (between $2.4\text{--}2.8 \times 10$), in agreement with the four-valent character of An in the complexes and their strong electrostatic interactions with the anionic (DOTA)^{4−} ligand. Accordingly, the negative charge in DOTA is most significant on the carboxylate oxygens that interact with An. In fact, the dominant An–ligand interaction corresponds to this ionic one, as demonstrated also by the very low electron densities ($\rho(r)$), the positive Laplacian values of the electron density ($\nabla^2\rho(r)$), and close-to-zero total electronic energy densities ($H(r)$) at the An–O and An–N bond critical points (BCP), cf. Table 2.

The An charges decrease gradually from Th to Pu, corresponding to a slightly decreasing ionic character along the An row. The same gentle trend also appears in the increasing electron densities at the An–O BCP-s. The change of $\rho(r)$ at the An–N BCP-s is non-significant. The above data have close values in the An(DOTA) and An(DOTA)(H₂O) complexes, the An charges being marginally larger in the hydrate derivatives.

The ellipticities (ϵ) of the electron density distributions at the BCP-s of the An–O and An–N interactions with DOTA are between 0 and 0.1 (Table 2), indicating small π characters of these interactions. (As a reference, the ellipticity of the C=C bond in ethane is 0.33 [73].) The ϵ values of the coordination with H₂O are ca. twice larger, referring to a larger π character due to the better spatial availability of the two lone pairs of the H₂O oxygen.

The above discussed An charges are determined by the charge transfer (CT) from the ligands to the An⁴⁺ ions during complex formation. From the two ligands in the An(DOTA)(H₂O) complexes, the dominant CT occurs from DOTA due to the anionic character and multiple number (8) of the donor atoms. However, the CT is somewhat less in the An(DOTA)(H₂O) complexes as compared to An(DOTA) because of the larger donor–An distances (cf. Figure 2). Another characteristic feature is the gradual increase in the transferred charge from Th to Pu, implying a simultaneous increase in covalent bonding. The slope becomes slightly steeper between Np and Pu with respect to that between U and Np. This may be associated with the observed out-of-trend move of Pu towards the O donors in Figure 3. In contrast, the CT from the neutral H₂O ligand is marginal and nearly constant along the An row (cf. Figure 4).

Another important integral property from the QTAIM analysis is the delocalisation index (DI), which corresponds to the number of shared electrons between An and the donor atoms of the ligands. The DI values depicted in Figure 5 confirm the dominance of the An–O_{DOTA} interactions in the covalent bonding. These DI values suggest an An–O_{DOTA} covalent bond order of ca. 0.5–0.6, in good agreement with the Wiberg bond indices [72] (cf. Figure 5). The increasing trend from Th to Pu agrees qualitatively with that of the CT shown in Figure 4, as well as with literature examples on related An^{IV} complexes [74–76].

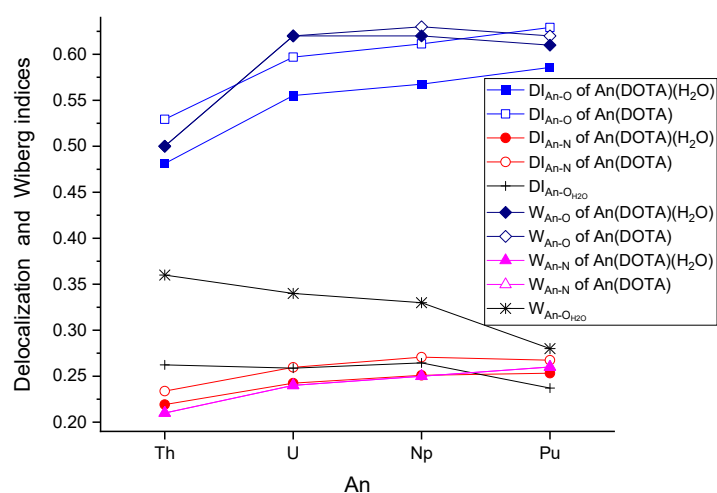


Figure 5. Delocalisation indices (DI, e) and Wiberg bond indices (W) of the An–O and An–N interactions. Due to the deformation from C₄ symmetry in the An(DOTA)(H₂O) structures, average values are depicted here. The individual values are given in Table S3 of the Supplementary Materials.

The shared electrons in the An–N_{DOTA} interactions amount to ca. half of those in the An–O_{DOTA} interactions. They also show a slight increase from Th to Pu, in good agreement with the related Wiberg indices.

Despite the marginal charge transfer from the neutral H₂O ligand to An, both the number of shared electrons and the Wiberg bond indices indicate significant An–O_{H₂O} covalent interactions in the An(DOTA)(H₂O) complexes (cf. Figures 4 and 5). The DI values are comparable, whereas the Wiberg bond indices are somewhat larger than those of the An–N_{DOTA} interactions, and they decrease from Th to Pu. The decreasing feature does not correlate with the nearly constant An–O_{H₂O} distances in Figure 2; however, it can be rationalised by appealing to the decreasing overlap due to the contracting An valence orbitals across the An row, whereas the distance depends on the competing bonding and steric interactions.

The natural orbital of chemical valence (NOCV) analysis [26] provides further details on the metal–ligand interactions in the complexes. Figure 6 shows NOCV orbital pairs representing the most significant DOTA → An donations in Th(DOTA). Relevant Kohn–Sham orbitals are depicted in Figure S1 in the Supplementary Materials. Whereas the NOCV picture demonstrates the charge accumulation and depletion in the bonding space and DOTA, respectively, in terms of Kohn–Sham orbitals, the metal–ligand interactions are extensively mixed with other intra-DOTA orbital interactions. In all the shown metal–ligand interactions, Th participates with hybrid 6d/5f atomic orbitals, in most cases with 6d major contributions.

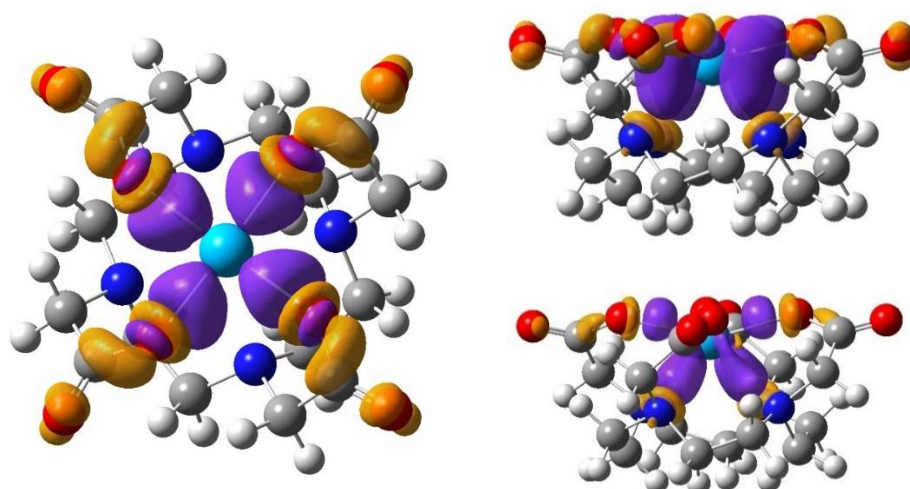


Figure 6. NOCV orbital pairs representing the most significant DOTA → An donations in Th(DOTA). (Left): O_{DOTA} → Th; (right): O/N_{DOTA} → Th. The colours yellow and violet indicate charge depletion and accumulation, respectively, with respect to the reference isolated fragments DOTA^{4−} and Th⁴⁺.

3.4. DOTA Complexes of An^{IV} vs. An^{III}

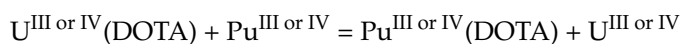
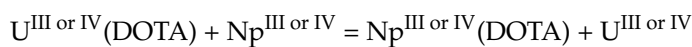
Molecular properties of An^{III}(DOTA) and An^{III}(DOTA)(H₂O) complexes obtained by DFT and multireference calculations have been published recently (An = Ac, U, Np, Pu, Am, Cm, Cf in [19], An = Ac in [77]). It should be noted that the present study was performed at a somewhat different theoretical level using small-core pseudopotentials in contrast to large-core ones (due to technical issues) in Ref. [19]. Yet, a qualitative comparison is feasible, and it led to the following conclusions:

There are significant differences between the complexes formed with An^{III} and An^{IV}:

1. An^{III} forms structures with TSAP conformation of DOTA, whereas An^{IV} forms structures with the SAP confirmation.
2. The donor–acceptor distances are considerably shorter with An^{IV}, because the stronger electrostatic interactions with the An⁴⁺ vs. An³⁺ metal ions pull the interacting species closer to each other (cf. Table S4 in the Supplementary Materials). Another

consequence of the higher positive charge of An^{IV} is the larger ligand → An charge transfer, yet the An charges still remain higher in the An^{IV} than in the An^{III} complexes.

3. The exchange reactions



with tri- or tetravalent An resulted in larger stabilities of the An^{IV} complexes and in a stability order of U < Np < Pu for both An oxidation states with reaction energies in terms of ΔG° of -44.6 , -85.4 , -85.8 , and -204.0 kJ/mol for Np^{III}, Pu^{III}, Np^{IV}, and Pu^{IV}, respectively. (Note that in the evaluation of ΔG° by Gaussian09, the electronic contributions are neglected.) The related values in terms of electronic energies at 0 K are -45.4 , -86.9 , -84.1 , and -204.8 kJ/mol, respectively.

4. Similarly, in terms of the QTAIM metrics, the trend for the strength of covalent interactions is the same (U < Np < Pu) for both An oxidation states, the interaction being significantly stronger in the An^{IV} complexes.

4. Conclusions

The DOTA ligand forms stable symmetric (C_4) complexes with the studied tetravalent actinides (An = Th, U, Np, Pu). The ground electronic states of the complexes agree with those of the An⁴⁺ ions. The 5f populations are well-reproduced in the lowest-energy states obtained by the DFT calculations, suggesting the applicability of DFT for such complexes.

The major An–ligand bonding interaction is the ionic one. Charge transfer from the ligands to the 6d (major) and 5f (minor acceptor) atomic An orbitals and the electron sharing that consequently occurs constitute the covalent bonding in the complexes. The latter interactions could be quantitatively analysed using the atomic charges and delocalisation indices from QTAIM analysis. In terms of these electronic properties, the covalent interactions increase gradually as Th < U < Np < Pu in both the An(DOTA) and An(DOTA)(H₂O) complexes. This increasing stability across the An row is in line with results on An complexes with other chelating ligands [78–80].

The secondary H₂O ligand distorted the C_4 structure and introduced notable changes in the molecular properties. As the bonding properties (An–ligand distances, CT, DI) indicate, this slightly weakened the An–DOTA interactions with respect to the parent complexes.

The larger stability of An^{IV}(DOTA) complexes that was found with respect to the An^{III} complexes suggests their more favourable practical applications.

Supplementary Materials: The following supporting information can be downloaded at: <https://www.mdpi.com/article/10.3390/sym14112451/s1>, Table S1: Selected computed and experimental An–O and An–N bond distances (Å) of An^{IV}(DOTA) complexes; Table S2: Selected computed geometrical characteristics of the An(DOTA) and An(DOTA)(H₂O) complexes; Table S3: (a) Integral properties of the electron density distribution (ρ) in the An(DOTA) and An(DOTA)(H₂O) complexes, (b) Selected results (au) from the DFT-based QTAIM analysis of An(DOTA) and An(DOTA)(H₂O) complexes; Table S4: Comparison of selected computed An–O and An–N bond distances (Å) of An^{IV} and An^{III}(DOTA) complexes; Figure S1: Selected molecular orbitals of Th(DOTA) with significant metal–ligand bonding. Cartesian coordinates of the optimised An(DOTA) and An(DOTA)(H₂O) complexes.

Funding: This research received no external funding.

Institutional Review Board Statement: Not applicable.

Informed Consent Statement: Not applicable.

Data Availability Statement: Not applicable.

Conflicts of Interest: The author declares no conflict of interest.

References

1. Viola-Villegas, N.; Doyle, R.P. The coordination chemistry of 1,4,7,10-tetraazacyclododecane-N,N',N'',N'''-tetraacetic acid (H₄DOTA): Structural overview and analyses on structure-stability relationships. *Coord. Chem. Rev.* **2009**, *253*, 1906–1925. [[CrossRef](#)]
2. Magerstädt, M.; Gansow, O.A.; Brechbiel, M.W.; Colcher, D.; Baltzer, L.; Knop, R.H.; Girton, M.E.; Naegelé, M. Gd(DOTA): An alternative to Gd(DTPA) as a T_{1,2} relaxation agent for NMR imaging or spectroscopy. *Magn. Reson. Med.* **1986**, *3*, 808–812. [[CrossRef](#)] [[PubMed](#)]
3. Chapon, C.; Lemaire, L.; Franconi, F.; Marescaux, L.; Legras, P.; Denizot, B.; Le Jeune, J.-J. Assessment of myocardial viability in rats: Evaluation of a new method using superparamagnetic iron oxide nanoparticles and Gd-DOTA at high magnetic field. *Magn. Reson. Med.* **2004**, *52*, 932–936. [[CrossRef](#)]
4. Zhang, S.; Trokowsky, R.; Sherry, A.D. A Paramagnetic CEST Agent for Imaging Glucose by MRI. *J. Am. Chem. Soc.* **2003**, *125*, 15288–15289. [[CrossRef](#)] [[PubMed](#)]
5. Chauvin, T.; Durand, P.; Bernier, M.; Meudal, H.; Doan, B.-T.; Noury, F.; Badet, B.; Beloeil, J.-C.; Tóth, É. Detection of Enzymatic Activity by PARACEST MRI: A General Approach to Target a Large Variety of Enzymes. *Angew. Chem. Int. Ed.* **2008**, *47*, 4370–4372. [[CrossRef](#)] [[PubMed](#)]
6. Yoo, B.; Pagel, M.D. A PARACEST MRI Contrast Agent To Detect Enzyme Activity. *J. Am. Chem. Soc.* **2006**, *128*, 14032–14033. [[CrossRef](#)]
7. Morgenstern, A.; Apostolidis, C.; Kratochwil, C.; Sathekge, M.; Krolicki, L.; Bruchertseifer, F. An overview of targeted alpha therapy with ²²⁵Actinium and ²¹³Bismuth. *Curr. Radiopharm.* **2018**, *11*, 200–208. [[CrossRef](#)]
8. Tafreshi, N.K.; Doligalski, M.L.; Tichacek, C.J.; Pandya, D.N.; Budzevich, M.M.; El-Haddad, G.; Khushalani, N.I.; Moros, E.G.; McLaughlin, M.L.; Wadas, T.J.; et al. Development of Targeted Alpha Particle Therapy for Solid Tumors. *Molecules* **2019**, *24*, 4314. [[CrossRef](#)]
9. Roscher, M.; Bakos, G.; Benešová, M. Atomic Nanogenerators in Targeted Alpha Therapies: Curie's Legacy in Modern Cancer Management. *Pharmaceuticals* **2020**, *13*, 76. [[CrossRef](#)]
10. Kratochwil, C.; Bruchertseifer, F.; Giesel, F.L.; Weis, M.; Verburg, F.A.; Mottaghy, F.; Kopka, K.; Apostolidis, C.; Haberkorn, U.; Morgenstern, A. ²²⁵Ac-PSMA-617 for PSMA-targeted α-radiation therapy of metastatic castration-resistant prostate cancer. *J. Nucl. Med.* **2016**, *57*, 1941–1944. [[CrossRef](#)]
11. Kratochwil, C.; Bruchertseifer, F.; Rathke, H.; Bronzel, M.; Apostolidis, C.; Weichert, W.; Haberkorn, U.; Giesel, F.L.; Morgenstern, A. Targeted α-therapy of metastatic castration-resistant prostate cancer with ²²⁵Ac-PSMA-617: Dosimetry estimate and empiric dose finding. *J. Nucl. Med.* **2017**, *58*, 1624–1631. [[CrossRef](#)] [[PubMed](#)]
12. Hammer, S.; Hagemann, U.B.; Zitzmann-Kolbe, S.; Larsen, A.; Ellingsen, C.; Geraudie, S.; Grant, D.; Indrevoll, B.; Smeets, R.; von Ahnen, O.; et al. Preclinical Efficacy of a PSMA-Targeted Thorium-227 Conjugate (PSMA-TTC), a Targeted Alpha Therapy for Prostate Cancer. *Clin. Cancer Res.* **2020**, *26*, 1985–1996. [[CrossRef](#)] [[PubMed](#)]
13. Jurcic, J.G.; Rosenblat, T.L.; McDevitt, M.R.; Pandit-Taskar, N.; Carrasquillo, J.A.; Chanel, S.M.; Ryan, C.; Frattini, M.G.; Cicic, D.; Larson, S.M.; et al. Phase I trial of the targeted alpha-particle nano-generator actinium-225 (²²⁵Ac-lintuzumab) (anti-CD33; HuM195) in acute myeloid leukemia (AML). *J. Clin. Oncol.* **2011**, *29*, 6516. [[CrossRef](#)]
14. Jurcic, J.G.; Ravandi, F.; Pagel, J.M.; Park, J.H.; Douglas Smith, B.; Douer, D.; Yair Levy, M.; Estey, E.; Kantarjian, H.M.; Earle, D.; et al. Phase I trial of α-particle therapy with actinium-225 (²²⁵Ac)-lintuzumab (anti-CD33) and low-dose cytarabine (LDAC) in older patients with untreated acute myeloid leukemia (AML). *J. Clin. Oncol.* **2015**, *33*, 7050. [[CrossRef](#)]
15. Kratochwil, C.; Bruchertseifer, F.; Giesel, F.; Apostolidis, C.; Haberkorn, U.; Morgenstern, A. Ac-225-DOTATOC—An Empiric Dose Finding for Alpha Particle Emitter Based Radionuclide Therapy of Neuroendocrine Tumors. *J. Nucl. Med.* **2015**, *56*, 1232.
16. Chakravarty, R.; Siamof, C.M.; Dash, A.; Cai, W. Targeted α-therapy of prostate cancer using radiolabeled PSMA inhibitors: A game changer in nuclear medicine. *Am. J. Nucl. Med. Mol. Imaging* **2018**, *8*, 247–267.
17. Kostelnik, T.I.; Orvig, C. Radioactive Main Group and Rare Earth Metals for Imaging and Therapy. *Chem. Rev.* **2019**, *119*, 902–956. [[CrossRef](#)]
18. Peters, J.A.; Djanashvili, K.; Geraldés, C.F.G.C.; Platas-Iglesias, C. The chemical consequences of the gradual decrease of the ionic radius along the Ln-series. *Coord. Chem. Rev.* **2020**, *406*, 213146. [[CrossRef](#)]
19. Kovács, A. Theoretical Study of Actinide(III)-DOTA Complexes. *ACS Omega* **2021**, *6*, 13321–13330. [[CrossRef](#)]
20. Tamain, C.; Dumas, T.; Hennig, C.; Guilbaud, P. Coordination of Tetravalent Actinides (An = Th^{IV}, U^{IV}, Np^{IV}, Pu^{IV}) with DOTA: From Dimers to Hexamers. *Chem. Eur. J.* **2017**, *23*, 6864–6875. [[CrossRef](#)]
21. Kent, G.T.; Wu, G.; Hayton, T.W. Synthesis and Crystallographic Characterization of the Tetravalent Actinide-DOTA Complexes [An^{IV}(k⁸-DOTA)(DMSO)] (An = Th, U). *Inorg. Chem.* **2019**, *58*, 8253–8256. [[CrossRef](#)] [[PubMed](#)]
22. Dovrat, G.; Illy, M.-C.; Berthon, C.; Lerner, A.; Mintz, M.H.; Maimon, E.; Vainer, R.; Ben-Eliyahu, Y.; Moiseev, Y.; Moisy, P.; et al. On the Aqueous Chemistry of the U^{IV}-DOTA Complex. *Chem. Eur. J.* **2020**, *26*, 3390–3403. [[CrossRef](#)] [[PubMed](#)]
23. Bader, R.F.W. *Atoms in Molecules. A Quantum Theory*; Oxford University Press: Oxford, UK, 1990.
24. Popelier, P.L.A. *Atoms in Molecules: An Introduction*; Prentice Hall: Harlow, UK, 2000.
25. Matta, C.F.; Boyd, R.J. An Introduction to the Quantum Theory of Atoms in Molecules. In *The Quantum Theory of Atoms in Molecules*; Matta, C.F., Boyd, R.J., Eds.; Wiley-VCH: Weinheim, Germany, 2007; pp. 1–34. [[CrossRef](#)]

26. Mitoraj, M.P.; Michalak, A.; Ziegler, T. A Combined Charge and Energy Decomposition Scheme for Bond Analysis. *J. Chem. Theor. Comput.* **2009**, *5*, 962–975. [[CrossRef](#)] [[PubMed](#)]
27. Frisch, M.J.; Trucks, G.W.; Schlegel, H.B.; Scuseria, G.E.; Robb, M.A.; Cheeseman, J.R.; Scalmani, G.; Barone, V.; Mennucci, B.; Petersson, G.A.; et al. *Gaussian 09, Revision D.01*; Gaussian, Inc.: Wallingford, CT, USA, 2010.
28. Regueiro-Figueroa, M.; Esteban-Gómez, D.; de Blas, A.; Rodríguez-Blas, T.; Platas-Iglesias, C. Understanding Stability Trends along the Lanthanide Series. *Chem. Eur. J.* **2014**, *20*, 3974–3981. [[CrossRef](#)] [[PubMed](#)]
29. Roca-Sabio, A.; Regueiro-Figueroa, M.; Esteban-Gómez, D.; de Blas, A.; Rodríguez-Blas, T.; Platas-Iglesias, C. Density functional dependence of molecular geometries in lanthanide(III) complexes relevant to bioanalytical and biomedical applications. *Comput. Theor. Chem.* **2012**, *999*, 93–104. [[CrossRef](#)]
30. Thiele, N.A.; Woods, J.J.; Wilson, J.J. Implementing f-Block Metal Ions in Medicine: Tuning the Size Selectivity of Expanded Macrocycles. *Inorg. Chem.* **2019**, *58*, 10483–10500. [[CrossRef](#)]
31. Kovács, A. Theoretical Study of Actinide Complexes with Macropa. *ACS Omega* **2020**, *5*, 26431–26440. [[CrossRef](#)]
32. Tao, J.; Perdew, J.P.; Staroverov, V.N.; Scuseria, G.E. Climbing the density functional ladder: Nonempirical meta-generalized gradient approximation designed for molecules and solids (TPSSTPSS). *Phys. Rev. Lett.* **2003**, *91*, 146401. [[CrossRef](#)]
33. Küchle, W.; Dolg, M.; Stoll, H.; Preuss, H. Energy-Adjusted Pseudopotentials for the Actinides. Parameter Sets and Test Calculations for Thorium and Thorium Monoxide. *J. Chem. Phys.* **1994**, *100*, 7535–7542. [[CrossRef](#)]
34. Cao, X.; Dolg, M.; Stoll, H. Valence basis sets for relativistic energy-consistent small-core actinide pseudopotentials. *J. Chem. Phys.* **2003**, *118*, 487–496. [[CrossRef](#)]
35. Cao, X.; Dolg, M. Segmented contraction scheme for small-core actinide pseudopotential basis sets. *J. Mol. Struct. (Theochem)* **2004**, *673*, 203–209. [[CrossRef](#)]
36. Moritz, A.; Cao, X.; Dolg, M. Quasirelativistic energy-consistent 5f-in-core pseudopotentials for divalent and tetravalent actinide elements. *Theor. Chem. Acc.* **2007**, *118*, 845–854. [[CrossRef](#)]
37. Grimme, S.; Ehrlich, S.; Goerigk, L. Effect of the damping function in dispersion corrected density functional theory. *J. Comp. Chem.* **2011**, *32*, 1456–1465. [[CrossRef](#)] [[PubMed](#)]
38. Roos, B.O. *Advances in Chemical Physics, Ab Initio Methods in Quantum Chemistry—II*; Lawley, K.P., Ed.; John Wiley & Sons Ltd.: Chichester, UK, 1987; pp. 399–446.
39. Karlström, G.; Lindh, R.; Malmqvist, P.-Å.; Roos, B.O.; Ryde, U.; Veryazov, V.; Widmark, P.-O.; Cossi, M.; Schimmelpfennig, B.; Neogrady, P.; et al. MOLCAS: A Program Package for Computational Chemistry. *Comput. Mat. Sci.* **2003**, *28*, 222–239. [[CrossRef](#)]
40. Aquilante, F.; Autschbach, J.; Carlson, R.K.; Chibotaru, L.F.; Delcey, M.G.; De Vico, L.; Galván, I.F.; Ferré, N.; Frutos, L.M.; Gagliardi, L.; et al. MOLCAS 8: New Capabilities for Multiconfigurational Quantum Chemical Calculations Across the Periodic Table. *J. Comput. Chem.* **2016**, *37*, 506–541. [[CrossRef](#)]
41. Douglas, N.; Kroll, N.M. Quantum Electrodynamical Corrections to the Fine Structure of Helium. *Ann. Phys.* **1974**, *82*, 89–155. [[CrossRef](#)]
42. Hess, B.A. Relativistic Electronic-Structure Calculations Employing a Two-Component No-Pair Formalism with External-Field Projection Operators. *Phys. Rev. A* **1986**, *33*, 3742–3748. [[CrossRef](#)]
43. Roos, B.O.; Lindh, R.; Malmqvist, P.-Å.; Veryazov, V.; Widmark, P.-O. New Relativistic ANO Basis Sets for Actinide Atoms. *Chem. Phys. Lett.* **2005**, *409*, 295–299. [[CrossRef](#)]
44. Widmark, P.-O.; Malmqvist, P.-A.; Roos, B.O. Density matrix averaged atomic natural orbital (ANO) basis sets for correlated molecular wave functions. *Theor. Chim. Acta* **1990**, *77*, 291–306. [[CrossRef](#)]
45. Roos, B.O.; Lindh, R.; Malmqvist, P.-Å.; Veryazov, V.; Widmark, P.-O. Main Group Atoms and Dimers Studied with a New Relativistic ANO Basis Set. *J. Phys. Chem. A* **2004**, *108*, 2851–2858. [[CrossRef](#)]
46. Roos, B.O.; Malmqvist, P.-Å. Relativistic Quantum Chemistry: The Multiconfigurational Approach. *Phys. Chem. Chem. Phys.* **2004**, *6*, 2919–2927. [[CrossRef](#)]
47. Lu, T.; Chen, F. Multiwfn: A multifunctional wavefunction analyzer. *J. Comput. Chem.* **2012**, *33*, 580–592. [[CrossRef](#)] [[PubMed](#)]
48. Spirlet, M.R.; Rebizant, J.; Desreux, J.F.; Loncin, M.F. Crystal and molecular structure of sodium aqua(1,4,7,10-tetraazacyclododecane-1,4,7,10-tetraacetato)europate(III) tetrahydrate $\text{Na}^+(\text{EuDOTA} \cdot \text{H}_2\text{O})^- \cdot 4\text{H}_2\text{O}$, and its relevance to NMR studies of the conformational behavior of the lanthanide complexes formed by the macrocyclic ligand DOTA. *Inorg. Chem.* **1984**, *23*, 359–363. [[CrossRef](#)]
49. Benetollo, F.; Bombieri, G.; Calabi, L.; Aime, S.; Botta, M. Structural Variations Across the Lanthanide Series of Macrocyclic DOTA Complexes: Insights into the Design of Contrast Agents for Magnetic Resonance Imaging. *Inorg. Chem.* **2003**, *42*, 148–157. [[CrossRef](#)] [[PubMed](#)]
50. Chang, C.A.; Francesconi, L.C.; Malley, M.F.; Kumar, K.; Gougoutas, J.Z.; Tweedle, M.F.; Lee, D.W.; Wilson, L.J. Synthesis, characterization, and crystal structures of $\text{M}(\text{DO3A})$ ($\text{M} = \text{iron, gadolinium}$) and $\text{Na}[\text{M}(\text{DOTA})]$ ($\text{M} = \text{Fe, yttrium, Gd}$). *Inorg. Chem.* **1993**, *32*, 3501–3508. [[CrossRef](#)]
51. Aime, S.; Barge, A.; Botta, M.; Fasano, M.; Danilo, A.J.; Bombieri, G. Crystal structure and solution dynamics of the lutetium(III) chelate of DOTA. *Inorg. Chim. Acta* **1996**, *246*, 423–429. [[CrossRef](#)]

52. Parker, D.; Pulukkody, K.; Smith, F.C.; Batsanov, A.; Howard, J.A.K. Structures of the yttrium complexes of 1,4,7,10-tetraazacyclododecane-N,N',N'',N'''-tetraacetic acid (H₄dota) and N,N''-bis(benzylcarbamoylmethyl)diethylenetriamine-N,N',N''-triacetic acid and the solution structure of a zirconium complex of H₄dota. *J. Chem. Soc. Dalton Trans.* **1994**, 689–693. [[CrossRef](#)]
53. Benetollo, F.; Bombieri, G.; Aime, S.; Botta, M. A holmium complex of a macrocyclic ligand (DOTA) and its isostructural europium analogue. *Acta Cryst. C* **1999**, *55*, 353–356. [[CrossRef](#)]
54. Burai, L.; Tóth, E.; Moreau, G.; Sour, A.; Scopelliti, R.; Merbach, A.E. Novel macrocyclic Eu^{II} complexes: Fast water exchange related to an extreme M-O_{water} distance. *Chem. Eur. J.* **2003**, *9*, 1394–1404. [[CrossRef](#)]
55. Aime, S.; Barge, A.; Benetollo, F.; Bombieri, G.; Botta, M.; Uggeri, F. A Novel Compound in the Lanthanide(III) DOTA Series. X-ray Crystal and Molecular Structure of the Complex Na[La(DOTA)La(HDOTA)]·10H₂O. *Inorg. Chem.* **1997**, *36*, 4287–4289. [[CrossRef](#)]
56. Anderson, O.P.; Reibenspies, J.H. [Ca(OH₂)₃[Ca(DOTA)]·7.7H₂O]_n. *Acta Cryst. C* **1996**, *52*, 792–795. [[CrossRef](#)]
57. Csajbók, É.; Baranyai, Z.; Bányai, I.; Brucher, E.; Király, R.; Müller-Fahnow, A.; Platzek, J.; Raduchel, B.; Schäfer, M. Equilibrium, ¹H and ¹³C NMR spectroscopy, and X-ray diffraction studies on the complexes Bi(DOTA)[−] and Bi(DO₃A-Bu). *Inorg. Chem.* **2003**, *42*, 2342–2349. [[CrossRef](#)] [[PubMed](#)]
58. Riesen, A.; Zehnder, M.; Kaden, T.A. Metal complexes of macrocyclic ligands. Part XXIII. Synthesis, properties, and structures of mononuclear complexes with 12- and 14-membered tetraazamacrocyclic-N,N',N'',N'''-tetraacetic acids. *Helv. Chim. Acta* **1986**, *69*, 2067–2073. [[CrossRef](#)]
59. Riesen, A.; Zehnder, M.; Kaden, T.A. Structures of two Zn²⁺ complexes with two tetraaza macrocyclic tetraacetates. *Acta Cryst. C* **1991**, *47*, 531–533. [[CrossRef](#)]
60. Heppeler, A.; André, J.P.; Buschmann, I.; Wang, X.; Reubi, J.-C.; Hennig, M.; Kaden, T.A.; Maecke, H.R. Metal-ion-dependent biological properties of a chelator-derived somatostatin analogue for tumour targeting. *Chem. Eur. J.* **2008**, *14*, 3026–3034. [[CrossRef](#)] [[PubMed](#)]
61. Dubost, J.P.; Leger, J.M.; Langlois, M.H.; Meyer, D.; Schaefer, M. Structure d'un agent de contraste utilisé en imagerie de résonance magnétique le complexe DOTA Gd, C₁₆H₂₄N₄O₈NaGd, 5H₂O. *C. R. Acad. Sci. Ser. II Mec. Phys. Chim. Sci. Terre Univers.* **1991**, *312*, 349–354.
62. Desreux, J.F. Nuclear magnetic resonance spectroscopy of lanthanide complexes with a tetraacetic tetraaza macrocycle. Unusual conformation properties. *Inorg. Chem.* **1980**, *19*, 1319–1324. [[CrossRef](#)]
63. Aime, S.; Botta, M.; Ermondi, G. NMR study of solution structures and dynamics of lanthanide(III) complexes of DOTA. *Inorg. Chem.* **1992**, *31*, 4291–4299. [[CrossRef](#)]
64. Hoeft, S.; Roth, K. Struktur und Dynamik von Lanthanoid-Tetraazacyclododecantetraacetat-(DOTA[−]) Komplexen in Lösung. *Chem. Ber.* **1993**, *126*, 869–873. [[CrossRef](#)]
65. Aime, S.; Botta, M.; Fasano, M.; Marques, M.P.; Geraldes, C.F.; Pubanz, D.; Merbach, A.E. Conformational and Coordination Equilibria on DOTA Complexes of Lanthanide Metal Ions in Aqueous Solution Studied by ¹H-NMR Spectroscopy. *Inorg. Chem.* **1997**, *36*, 2059–2068. [[CrossRef](#)]
66. Wilson, J.J.; Ferrier, M.; Radchenko, V.; Maassen, J.R.; Engle, J.W.; Batista, E.R.; Martin, R.L.; Nortier, F.M.; Fassbender, M.E.; John, K.D.; et al. Evaluation of nitrogen-rich macrocyclic ligands for the chelation of therapeutic bismuth radioisotopes. *Nucl. Med. Biol.* **2015**, *42*, 428–438. [[CrossRef](#)] [[PubMed](#)]
67. Khabibullin, A.R.; Karolak, A.; Budzevich, M.M.; McLaughlin, M.L.; Morse, D.L.; Woods, L.M. Structure and properties of DOTA-chelated radiopharmaceuticals within the ²²⁵Ac decay pathway. *MedChemComm* **2018**, *9*, 1155–1163. [[CrossRef](#)] [[PubMed](#)]
68. Shannon, R.D. Revised Effective Ionic Radii and Systematic Studies of Interatomic Distances in Halides and Chalcogenides. *Acta Cryst.* **1976**, *A32*, 751–767. [[CrossRef](#)]
69. Carnall, W.T.; Crosswhite, H.M. Optical Spectra and Electronic Structure of Actinide Ions in Compounds and in Solution. In *The Chemistry of the Actinide Elements: Volume 2*; Katz, J.J., Seaborg, G.T., Morss, L.R., Eds.; Springer: Dordrecht, The Netherlands, 1986; pp. 1235–1277. [[CrossRef](#)]
70. Worden, E.F.; Blaise, J.; Fred, M.; Trautmann, N.; Wyart, J.-F. Spectra and Electronic Structures of Free Actinide Atoms and Ions. In *The Chemistry of the Actinide and Transactinide Elements*; Morss, L.R., Edelstein, N.M., Fuger, J., Eds.; Springer: Dordrecht, The Netherlands, 2006; pp. 1836–1892. [[CrossRef](#)]
71. Rodrigues, G.C.; Indelicato, P.; Santos, J.P.; Patté, P.; Parente, F. Systematic calculation of total atomic energies of ground state configurations. *At. Data Nucl. Data Tables* **2004**, *86*, 117–233. [[CrossRef](#)]
72. Wiberg, K.B. Application of the pople-santry-segal CNDO method to the cyclopropylcarbanyl and cyclobutyl cation and to bicyclobutane. *Tetrahedron* **1968**, *24*, 1083–1096. [[CrossRef](#)]
73. Silva Lopez, C.; de Lera, A.R. Bond Ellipticity as a Measure of Electron Delocalization in Structure and Reactivity. *Curr. Org. Chem.* **2011**, *15*, 3576–3593. [[CrossRef](#)]
74. Kerridge, A. f-Orbital covalency in the actinocenes (An = Th–Cm): Multiconfigurational studies and topological analysis. *RSC Adv.* **2014**, *4*, 12078–12086. [[CrossRef](#)]
75. Kerridge, A. Quantification of f-element covalency through analysis of the electron density: Insights from simulation. *Chem. Commun.* **2017**, *53*, 6685–6695. [[CrossRef](#)]

76. Radoske, T.; März, J.; Patzschke, M.; Kaden, P.; Walter, O.; Schmidt, M.; Stumpf, T. Bonding Trends in Tetravalent Th–Pu Monosalen Complexes. *Chem. Eur. J.* **2020**, *26*, 16853–16859. [[CrossRef](#)]
77. Kovács, A.; Varga, Z. Metal–ligand interactions in complexes of cyclen-based ligands with Bi and Ac. *Struct. Chem.* **2021**, *32*, 1719–1731. [[CrossRef](#)]
78. Kelley, M.P.; Su, J.; Urban, M.; Luckey, M.; Batista, E.R.; Yang, P.; Shafer, J.C. On the Origin of Covalent Bonding in Heavy Actinides. *J. Am. Chem. Soc.* **2017**, *139*, 9901–9908. [[CrossRef](#)] [[PubMed](#)]
79. Kelley, M.P.; Deblonde, G.J.P.; Su, J.; Booth, C.H.; Abergel, R.J.; Batista, E.R.; Yang, P. Bond Covalency and Oxidation State of Actinide Ions Complexed with Therapeutic Chelating Agent 3,4,3-LI(1,2-HOPO). *Inorg. Chem.* **2018**, *57*, 5352–5363. [[CrossRef](#)] [[PubMed](#)]
80. Chandrasekar, A.; Ghanty, T.K. Uncovering Heavy Actinide Covalency: Implications for Minor Actinide Partitioning. *Inorg. Chem.* **2019**, *58*, 3744–3753. [[CrossRef](#)] [[PubMed](#)]